

## A 0.5 mm<sup>2</sup> 7-MHZ CAPACITIVE BULK ACOUSTIC WAVE GYROSCOPE IN (100) SILICON WITH LARGE DYNAMIC RANGE

*Amir Rahafrooz<sup>1</sup>, Diego E. Serrano<sup>1</sup>, Duane Younkin<sup>1</sup>, Shin Nagpal<sup>1</sup>, Ijaz Jafri<sup>1</sup> and Farrokh Ayazi<sup>1,2</sup>*

<sup>1</sup>Qualtré Inc., Marlborough, MA, USA

<sup>2</sup>Georgia Institute of Technology, Atlanta, GA, USA

## ABSTRACT

This paper presents, what is to the authors' knowledge, the smallest MEMS gyroscope reported to date. With a footprint of only  $0.5 \text{ mm}^2$ , the device consists of a high frequency bulk acoustic wave (BAW) disk resonator (408  $\mu\text{m}$  diameter) with robust performance to environmental disturbances, and a large dynamic range of more than 6,000 °/s. The device utilizes nano-transduction capacitive gaps provided by the HARPSS process, which enable an extremely small footprint without sacrificing other specifications, such as sensitivity and noise. Moreover, due to the inherently stiff structure, the presented BAW gyro has a significantly reduced sensitivity to shock and vibration [1]. The device exhibits a measured angle-random walk (ARW) of  $1 \text{ }^\circ/\sqrt{\text{h}}$  and a bias instability of  $15 \text{ }^\circ/\text{h}$ , which are dominated by the thermal and flicker noise of the interface electronics. The gyro element itself is capable of reaching 5-10X lower noise levels.

## INTRODUCTION

In recent years, new applications such as pedestrian and drone navigation have further restricted the die-size requirements and the sensitivity to shock and vibrations in MEMS gyros. However, most of the commercially-available gyros consist of low-frequency tuning-fork-based devices, which are intrinsically prone to linear acceleration. Efforts to improve the performance of such devices usually lead to having larger structures, making them unsuitable candidates for cost sensitive applications. For instance, consumer-grade 3-axis gyros can have MEMS surface areas as small as  $1.5 \text{ mm}^2$  per axis, but their noise-floor can degrade by up to 1000X in the presence of a random linear acceleration [2, 3]. Moreover, single-axis industrial-grade MEMS gyros with improved vibration performance are also commercially available, but their acceleration-rejection schemes require large redundant proof-masses, making their surface-area as large as about  $18 \text{ mm}^2$  [4]. On the other hand, the solid-state nature of BAW resonators [5] makes them inherently immune to shock and vibration disturbances, which in combination with nanometer-scale capacitive gaps [6], enable the implementation of smaller gyros without sacrificing performance.

This paper presents a BAW disk resonator gyroscope design, which in combination with nanometer transduction gaps will allow for implementation of an environmentally-robust gyro in a very small die footprint ( $0.5 \text{ mm}^2$ ).

DESIGN AND MODELING

The resonant body of the gyroscope is comprised of an axis-symmetric disk resonator with outer radius of only

204  $\mu\text{m}$  implemented in (100) single crystalline silicon (SCS) (Fig 1.a), and isolated from the substrate by use of a novel decoupling structure.

## Decoupling Structure Design Considerations

The decoupling structure not only minimizes the device anchor loss to isolate the gyroscope from the substrate [2], but also provides a rigid support that guarantees robust performance across temperature, stress, shock and vibration disturbances. Thus, the lowest resonance modes of the structure that determine its robustness, are pushed higher in frequency (Fig 2). Additionally, such structure has been carefully designed to ensure that it would not introduce any spurious modes within the vicinity of the gyroscope modes of operation.

Figures 1.b & 1.c show the two degenerate third-elliptical in-plane modes with the resonance frequency of 7 MHz, which were used to configure the device as a rotation-rate gyro.

### **Electrode Configuration**

Electrostatic transduction with nanometer gaps of 190 nm was used to operate the gyroscope. Figures 1.b & 1.c show the utilized electrode configuration with respect to both drive and sense modes. The electrodes labeled in white and yellow align only with the displacement of one of the two modes controlling the operation of the drive and sense modes, respectively. On the other hand, the electrodes labeled in green are located between the two modes allowing for mode-to-mode decoupling.

Size and location of the single excitation ( $V_{DRV}$ ) and differential pick-off ( $I_{DRV+}$  &  $I_{DRV-}$ ) electrodes for the drive mode are carefully chosen to ensure that motional impedance of the in-plane spurious modes are higher in magnitude and have a different phase from the drive mode of operation of the gyro (Fig. 3). This is a necessary condition to provide stable drive-loop during operation of the gyro.

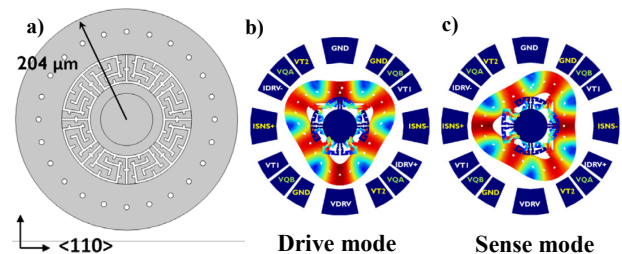


*Figure 1: (a) Schematic representation of the designed gyroscope. (b) & (c) Electrode configuration with respect to top view modal deformations of the two degenerate third-elliptical in-plane modes used as drive (b) and sense (c) modes. The electrodes labeled in white, yellow and green control the drive mode, sense mode and the mode-decoupling respectively*

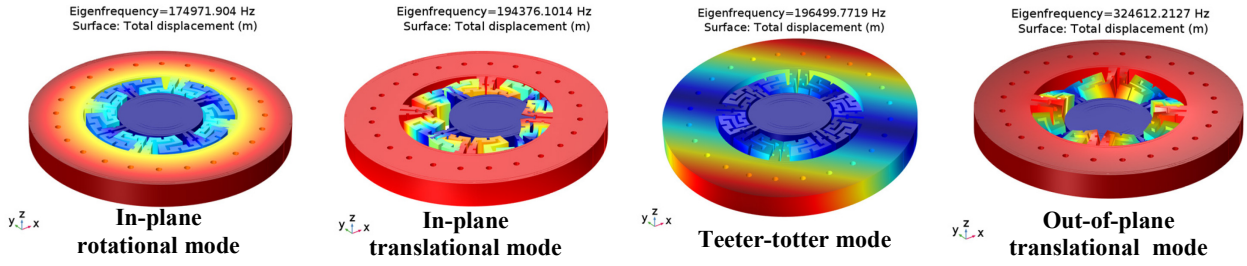


Figure 2: Modal deformation and resonance frequency for the lowest resonance modes of the gyroscope

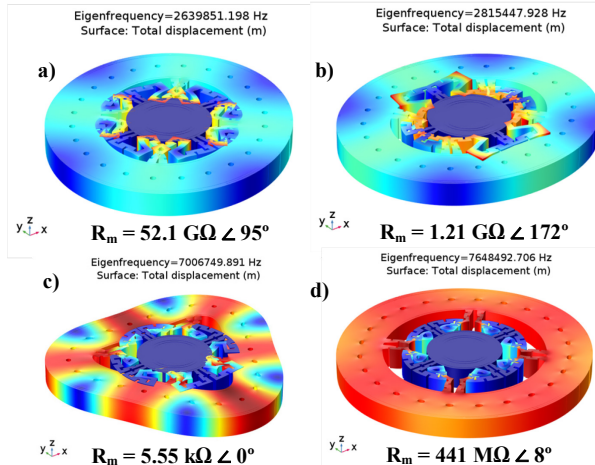


Figure 3: Simulated motional impedance ( $R_m$ ) of the drive loop for the two  $n=2$  in-plane elliptical modes (a & b), the drive mode (c) and the breathing mode (d).  $Q$  of 100,000 is used for all modes

### Quality Factor Design

A comprehensive energy loss analysis was performed using COMSOL Multiphysics. Support loss, Thermoelectric Damping (TED) and Squeezed/Sliding Film Damping (SFD) were simulated to predict the final quality factor of the gyro. Perfectly matched layers (PML) were used to model the support loss that resulted in  $Q_{\text{Support}}$  of 700 billion.  $Q_{\text{TED}}$  of 119,000 was obtained at room temperature that is being mainly limited by the decoupling structure and the release holes inside the annulus. Knowing the electrode configuration and gap size, SFD simulation was run at room temperature at different pressures. The total  $Q$  was then calculated using the following equation:  $1/Q_{\text{Total}} = (1/Q_{\text{Support}} + 1/Q_{\text{TED}} + 1/Q_{\text{SFD}})$ . Figure 4 shows the expected total quality factor of the gyroscope for both drive and sense modes across pressure at room temperature.

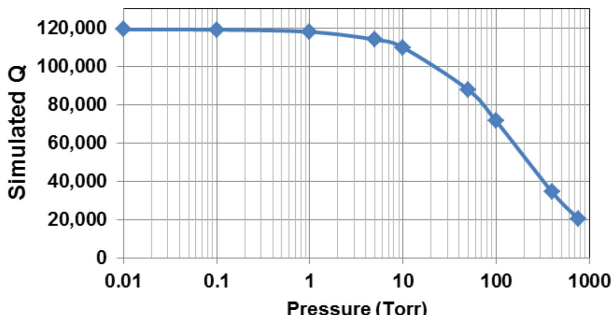


Figure 4: Total simulated quality factor over pressure with simulated  $Q_{\text{TED}} = 119,000$  and  $Q_{\text{Support}} = 700$  billion

## FABRICATION

Devices were fabricated on (100) silicon-on-insulator (SOI) wafers with device-layer thickness of 40  $\mu\text{m}$  and 2  $\mu\text{m}$  thick buried-oxide. A modified version of the high-aspect ratio poly- and single crystal silicon (HARPSS) process flow [5] was used to fabricate the gyros.

Figure 5 shows the final schematic cross-sectional view of the capped gyro. Trenches that define the gyro and electrode boundaries were created by DRIE etching of silicon. A 190 nm sacrificial thermal oxide was used to define the nanometer transduction gap. The gyros were released in HF acid. Lastly, the MEMS wafer is hermetically bonded to a capping wafer that is processed separately to provide final package pressure of 1-10 Torr.

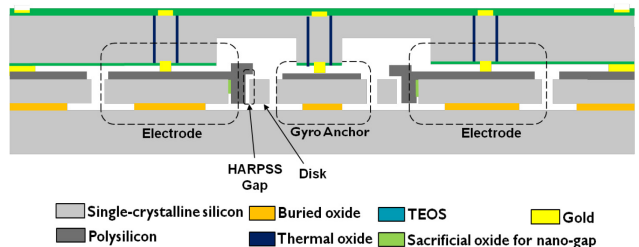


Figure 5: Schematic of a cross-sectional view of the capped single-crystalline silicon BAW Z-axis gyroscope utilizing a modified HARPSS process for fabrication.

Figure 6 shows the top SEM view of a fabricated gyro with a wafer-level packaged die size of 0.5  $\text{mm}^2$ .

## CHARACTERIZATION RESULTS

### Open-Loop Characterization

The fabricated gyroscopes were first characterized in an open-loop configuration using a network analyzer. Polarization voltage of 20 V was applied to the gyro. Figure 7 shows the frequency response of a gyro before and after mode-matching and mode-decoupling. With all the frequency tuning ( $V_{T1}$  &  $V_{T2}$ ) & mode decoupling ( $V_{QA}$  &  $V_{QB}$ ) voltages set to 0V (initial state), the drive mode was excited. The frequency response of the gyro for the drive and sense modes are shown in Figure 7a in blue and red colors respectively. The large red sense frequency response signal is the quadrature signal, implying that modes are strongly coupled and the initial frequency split between the two modes is 327 Hz. Mode-decoupling electrodes can be used to decouple the modes and remove the quadrature signal seen on the sense mode, and then the frequency tuning electrode can reduce the frequency split to zero. The frequency response of the same gyro after mode-decoupling and mode-matching is shown in Figure 7b.

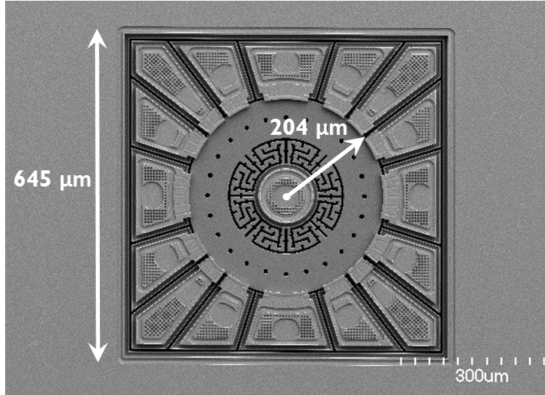


Figure 6: SEM view of the 7MHz SCS BAW gyroscope. The die size including the seal-ring for wafer level packaging is  $0.5 \text{ mm}^2$

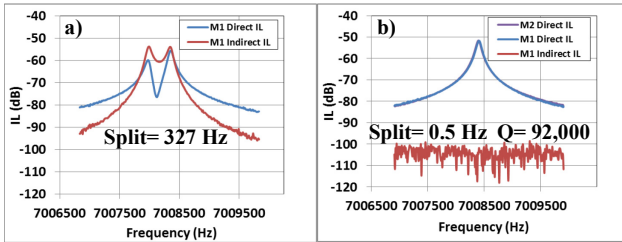


Figure 7: Open-loop frequency response of a gyro with drive and sense mode insertion losses in blue and red respectively: (a) Initial state with  $V_{QA}$ ,  $V_{QB}$ ,  $V_{T1}$  &  $V_{T2}$  are set to 0 V (b) Final state where  $V_Q$  &  $V_T$  electrodes are used to mode-decouple and mode-match the gyro

Figure 8 shows a color-map plot of the initial frequency split ( $(f_{\text{Drive}} - f_{\text{Sense}})/f_{\text{Drive}}$ ) of the gyros across two wafers. The pattern in the plot is being created due to fabrications imperfections. This mainly happens during lithography and DRIE steps to define and etch the trenches around the resonator body.

After mode-decoupling and mode-matching of gyros, quality factor across several wafers were measured.. Figure 9 shows the measured quality factor distribution for drive and sense modes. The variation on Q is believed to be mainly due to the change in package pressure across each wafer. The average measured Q of  $\sim 94,000$  closely matches the simulated Q value (Fig. 4) at 20 Torr, which is in fact the verified pressure inside package.

To further study the quality factor of the gyro, and how well the decoupling structure isolates the resonator

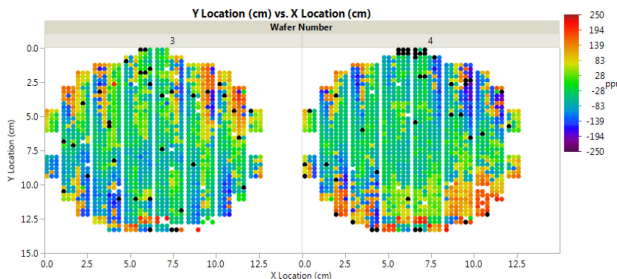


Figure 8: Initial frequency split color-map across two wafers showing a distribution of  $\pm 250$  parts per millions (ppm). All frequency tuning and mode-decoupling electrodes are set to 0 V for this measurement.

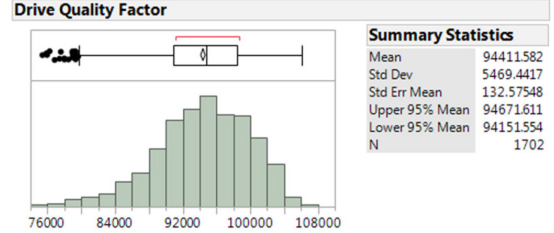


Figure 9: Measured drive & sense quality factor distribution across few wafers. Mean and Std. Dev. for the two distributions match closely.

body from the substrate, Q values of both drive and sense modes were measured across temperature (Fig 10). The Q values for both modes are monotonically changing across temperature, confirming a successful energy decoupling from the substrate [2].

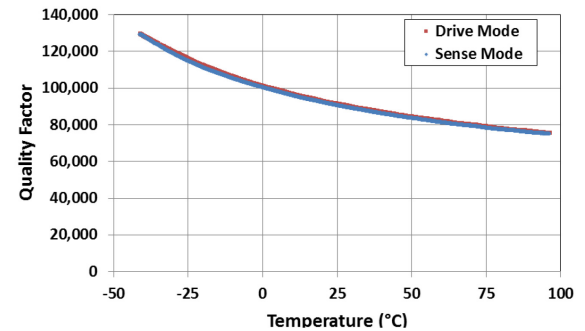


Figure 10: Measured Q of a gyro across temperature for both drive and sense modes confirming a successful energy decoupling from the substrate. Typical value for  $\Delta Q/Q$  is 0.025.

### Closed-Loop Operation

Singulated gyros were characterized in a closed-loop configuration (Fig. 11) by the use of external electronics (HF2LI from Zurich Instruments). The drive loop uses a Phase-Locked Loop (PLL) to track the phase at the resonance frequency of drive mode, ensuring oscillation at the resonance frequency. In addition Amplitude-Gain Controller (AGC) ensures that the drive amplitude of the drive mode is kept constant at  $1/10^{\text{th}}$  of the gap size to provide linearity. The output of the sense mode gets demodulated by a signal from the drive loop were its in-phase component is the rate out while the out of phase component should be zero for a mode-decoupled part. An automatic mode-decoupling scheme is implemented using a PID controller that adjusts the voltage on a decoupling electrode to drive the out-of-phase component of the Sense demodulator to zero.

The measured scale-factor of  $540 \mu\text{V}/(\text{°}/\text{s})$  agrees very well with the expected designed value (Fig 12). The expected mechanical noise-density for this device is 2.75

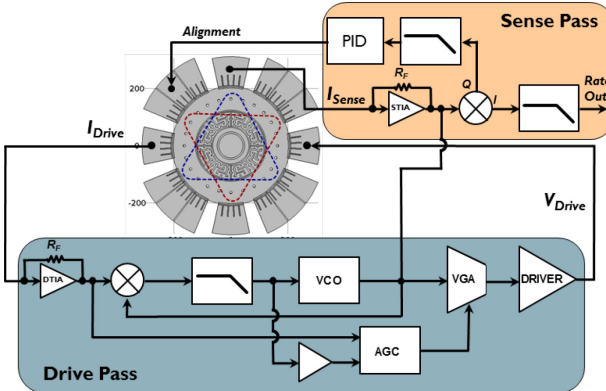


Figure 11: Schematic system-level representation of the gyroscope during closed-loop operation

$\text{m}(\text{s})/\sqrt{\text{Hz}}$ , which corresponds to an angle-random walk (ARW) of  $0.165 \text{ }^{\circ}/\text{h}$ . However, due to the limited input-referred noise of the external electronics, the measured noise-density is in the order of  $17 \text{ m}(\text{s})/\sqrt{\text{Hz}}$  (ARW =  $1 \text{ }^{\circ}/\text{h}$ ). This value can be easily reduced by the use of an integrated circuit.

Figure 13 shows the expected mechanical ARW for the designed gyroscope, and the measured Allan deviation plot with the use of external electronics. Lastly, Figure 14 compares the sensitivity to random vibration between this

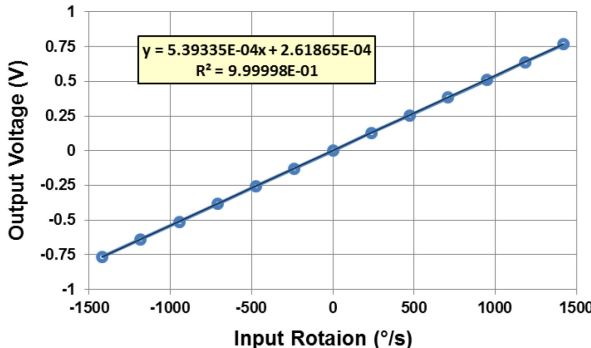


Figure 12: Output response of the gyro to rotation rate with measured non-linearity of 0.035 %, which is limited by the electronics. Applied rotation rate is limited by test equipment capability. Full scale range of the gyro is calculated to be  $\pm 6,300 \text{ }^{\circ}/\text{s}$  for 0.05% non-linearity.

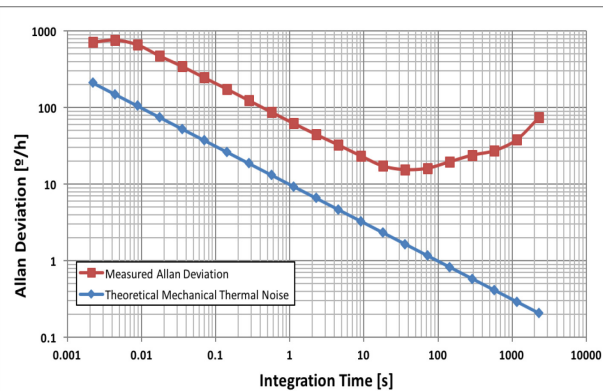


Figure 13: Allan deviation plot of the designed single crystalline silicon BAW gyroscope with ARW  $1 \text{ }^{\circ}/\text{hr}$  and Bias Instability of  $15 \text{ }^{\circ}/\text{hr}$

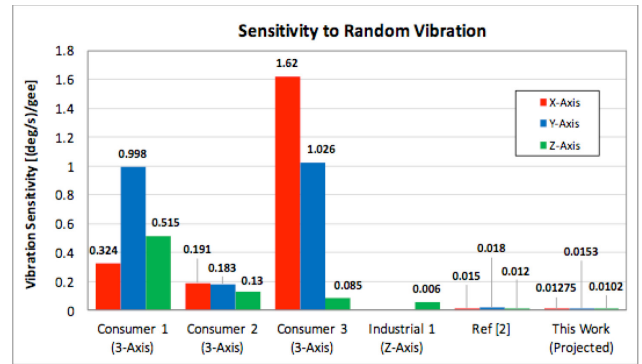


Figure 14: Sensitivity to random vibration comparing the measured values for three consumer & one industrial gyros with two BAW gyro designs (Ref [2] & This work) work and some commercially available MEMS gyroscopes.

## ACKNOWLEDGEMENTS

This work was supported in part by the Defense Advanced Research Projects Agency Microsystems Technology Office, Single-Chip Timing and Inertial Measurement Unit (TIMU) through SSC pacific contract # N66001-11-C-4176.

## REFERENCES

- [1] F. Ayazi, "Multi-DOF Inertial MEMS: From Gaming to Dead-Reckoning", *Transducers*, China, pp. 2805-2808, 2011
- [2] D. E Serrano et al, "Substrate-decoupled, bulk-acoustic wave gyroscopes: Design and evaluation of next-generation environmentally robust devices", *Microsystems & Nanoengineering* 2, Article number: 16015, 2016
- [3] D. E. Serrano et al., "Environmentally-robust high-performance tri-axial bulk acoustic wave gyroscopes," *2016 IEEE/ION Position, Location and Navigation Symposium (PLANS)*, Savannah, GA, 2016, pp. 5-8.
- [4] R. Colin Johnson, "ADI ups ante in high-precision MEMS gyros", [http://www.eetimes.com/document.asp?doc\\_id=1258816](http://www.eetimes.com/document.asp?doc_id=1258816), 2011
- [5] H. Johari and F. Ayazi, "Capacitive Bulk Acoustic Wave Silicon Disk Gyroscopes," *2006 International Electron Devices Meeting*, San Francisco, CA, 2006, pp. 513-516.
- [6] F. Ayazi, K. Najafi, "High Aspect-Ratio Combined Poly and Single-Crystal Silicon (HARPSS) MEMS Technology," *Journal of Microelectromechanical Systems*, vol. 9, pp. 288-294, 2000.

## CONTACTS

Amir Rahafrooz, tel: +1-303-963-657; [arahafrooz@ieee.org](mailto:arahafrooz@ieee.org)  
Farrokh Ayazi, tel: +1-404-894-9496; [ayazi@gatech.edu](mailto:ayazi@gatech.edu)